Synthesis of alpha-Al_2O_3 Template on Ni Superalloy Surface by Chemical Vapor Deposition

Y.-F. Su, M. Torzilli, J. D. Meyer, and W. Y. Lee
Department of Chemical, Biochemical, and Materials Engineering
Stevens Institute of Technology
Hoboken, NJ 07030

M. J. Lance and C. J. Rawn
Metals & Ceramics Division
Oak Ridge National Laboratory
Oak Ridge, TN 37831

S. Ruppi
SECO Tools AB
Fagersta, Sweden

Abstract

The life of thermal barrier coatings (TBCs) used in aircraft engine and power generation turbines is largely dictated by: (1) the ability of a metallic bond coating to form an adherent thermally grown oxide (TGO) at the metal-ceramic interface and (2) the rate at which the TGO grows upon oxidation. It is postulated that a thin α-Al_2O_3 template, if appropriately synthesized on a Ni-based alloy, will guide the alloy surface to form a TGO that is more tenacious and slower growing than what is attainable with state-of-the-art bond coatings. The feasibility of preparing such a template was examined using a chemical vapor deposition (CVD) process previously developed for cutting tool applications. A coating directly deposited by this method on a single crystal Ni superalloy substrate consisted of ~1 μm α-Al_2O_3 crystals in a matrix of amorphous Al_2O_3. The coating, although not entirely α-Al_2O_3, promoted the formation of a highly stressed and adherent TGO layer (-6.0 GPa) on the alloy surface upon subsequent oxidation. When the alloy surface was modified with an electroplated Pt layer, the coating was entirely α-Al_2O_3, but with the presence of fine microcracks on the coating surface. In comparison to results observed for pure Pt and Ni substrates, it appeared that the role of the Pt interlayer was to promote the formation of κ-Al_2O_3 nuclei, which subsequently transformed to α-Al_2O_3 during the CVD growth step. These results suggested that the nucleation and growth of a fully α-Al_2O_3 layer on the Ni superalloy surface, without forming microcracks, would be difficult through simple adaptation of the CVD process previously developed for the cutting tool industry.

Introduction

TBCs are currently used, in conjunction with air cooling, to prolong the life of metallic "hot-section" turbine components in revenue generating aircraft engine services.[1] State-of-the-art TBCs used for rotating airfoils in aircraft engines consist of a strain-tolerant Y_2O_3-stabilized ZrO_2 (YSZ) layer prepared by electron beam physical vapor deposition (EBPVD) and a metallic bond coating which provides high-temperature oxidation protection. It is recognized that, among various failure mechanisms observed, the principal failure mode of the EBPVD-TBCs is progressive fracture along the interface region between the metallic bond coating surface and its thermally grown oxide (TGO) upon oxidation and thermal cycling.[1-4] Bond coatings commonly used with the EBPVD-YSZ layer are: (1) MCrAlY (where M is Ni, Co, or NiCo) prepared by vacuum plasma spray (VPS)[1] and (2) Pt-aluminide prepared by Pt electroplating and subsequent aluminizing by pack cementation or chemical vapor deposition (CVD).[5]

There are some intriguing observations reported in the literature about enhancing the oxidative stability of the metal-ceramic interface by incorporating a thin-layer of high-quality Al_2O_3. As reported in his patent, Strangman[6] observed that the presence of an Al_2O_3 interlayer (~1 µm) prepared by CVD between NiCoCrAlY and EBPVD-YSZ increased the TBC's burner rig life by five-fold. The increased oxidation resistance was attributed to the dense morphological quality and high chemical purity of the CVD-Al_2O_3 layer, although the claims were made without substantial characterization results. Another independent study by Sun et al.[7] showed that the presence of a CVD Al_2O_3 layer (4 µm thick) between a plasma sprayed YSZ layer and a NiCoCrAlY layer substantially increased the cyclic oxidation life of the YSZ layer. The rate of bond coating oxidation was observed to be lower due to the presence of the artificial Al_2O_3 layer. It was also claimed that the formation of spinels (i.e., transient oxide phases that form during the initial stage of Ni alloy oxidation) was not observed at the YSZ-TGO interface.

Both Strangman and Sun et al. used a CVD process which utilizes $AlCl_3$, CO_2, and H_2 as precursors at a deposition temperature of ~1000°C. This chloride-based CVD process was previously developed, and is being widely used for the cutting tool industry.[8] The non-line of sight, atomistic growth technique is attractive for manufacturing, since engineering components with intricate shapes and complex surface features can be readily coated. The CVD process is the only technique currently capable of commercially producing α-Al_2O_3 in the form of coherent and dense coatings. PVD methods such as sputtering,[9] reactive sputtering,[10,11] reactive evaporation,[12] ion-assisted deposition,[13,14] and cathodic arc plasma deposition[15] are generally known to produce metastable or amorphous Al_2O_3, unless post-deposition annealing above 1000°C is applied.

In the cutting tool industry, WC/Co substrates are deposited with Ti(C,N) and Ti_2O_3 interlayers prior to the α-Al_2O_3 growth step. The Ti(C,N) interlayer is used as a diffusion barrier, since some of substrate elements and impurities (particularly Co) are found to cause the formation of metastable phases or undesired morphological features such as whiskers during the coating growth.[8] It has been postulated that the role of the Ti_2O_3 layer is to promote the preferential nucleation of α-Al_2O_3.[16] Another important processing feature is that air leaks into the CVD process must be tightly controlled in order to avoid the development of "cauliflower" growth morphology and powder formation in the gas phase. Despite these difficulties, remarkable engineering progress has been made with controlling the nucleation and growth behavior of Al_2O_3 on the cutting tool surface. For example, the selective growth of α-Al_2O_3 or κ-Al_2O_3 (even α-Al_2O_3/κ-Al_2O_3 multilayers) is possible by adding a small concentration (~ 0.1%) of $TiCl_4$ or $ZrCl_4$ as a dopant to the gas phase during the initial period of coating growth.[8,16]

In the present study, an industry standard CVD process, previously developed at SECO Tools for the cutting tool industry, was used to prepare α-Al_2O_3 coating specimens on the (100) surface of a single crystal Ni alloy (René N5) and on the same alloy coated with an electroplated Pt interlayer. The Pt-plated René N5 was investigated for the following reasons: (i) Pt may mitigate adverse effects of some alloying elements of the Ni alloy (particularly Co and Cr), which are known to cause the growth of Al_2O_3 whiskers;[8,17] (ii) beneficial effects of Pt on TGO adhesion are well known;[18,19] and (iii) Pt electroplating is a routine part of turbine coating production and repairing. While René N5 and Pt-plated René N5 substrates were of engineering importance for this study, pure Ni and Pt substrates were also used to study the nucleation and growth behavior of CVD-Al_2O_3 in the absence of impurity effects. Impurities such as Co and Cr on the substrate surface and chlorides of Si, Fe, Ni, Cr, and Co from the gas phase have been shown to influence both the morphology and phase content of CVD-Al_2O_3 coatings prepared for the cutting tool industry.[8,17,20,21]

Experimental

CVD-Al_2O_3 coating specimens were prepared at SECO Tools, Sweden, using the procedures described elsewhere [16,22,23], at a deposition temperature of ~1000°C and a reactor pressure of ~10 kPa with $AlCl_3$, CO_2 and H_2 as precursors. A single crystal Ni alloy (René N5; René is a trademark of General Electric Company, Fairfield, CT) was cast as a cylindrical rod with the [100] seed direction. The alloy rod was sliced radially to produce disc specimens (0.2 cm thickness x 1.2 cm diameter) while preserving the (100) orientation on the disc surface. The nominal composition (in weight %) of the alloy is: 6.2 Al, 0.05 C, 7.5 Co, 7.0 Cr, 0.16 Hf, 1.5 Mo, 3.0 Re, 6.5 Ta, 0.02 Ti, 5.0 W, and Ni as the balance. This alloy was melt-desulfurized to below 1 ppm sulfur by PCC Airfoils for Oak Ridge National Laboratory (ORNL), and its oxidation characteristics have been extensively studied as described elsewhere.[24,25] The specimen surface was polished prior to coating experiments with 0.05 µm Al_2O_3 suspension. General Electric Aircraft Engines provided René N5 discs (0.3 cm thickness x 2.5 cm diameter) electroplated with a layer of pure Pt. The thickness of the Pt layer was nominally ~7 µm. The Pt-coated alloy surface was not polished prior to the coating experiments. Pt and Ni substrates were cut to 10 x 10 mm squares from Pt and Ni foils (99.99+% for both foils, Goodfellow, Berwyn, PA). The Pt and Ni surfaces were not polished for the coating experiments.

Coating morphology and compositions were examined using a field emission scanning electron microscope (SEM, LEO 982, LEO Electron Microscopy Inc., Thornwood, NY) equipped with an energy dispersive spectrometer (EDS). Phase contents and microstructural orientation of coating specimens were studied by X-ray diffraction (XRD, Siemens Diffractometer D5000) with capability to perform grazing incidence (GIXRD) measurements. The GIXRD technique was used to analyze the coating layer while reducing contributions from substrate peaks, as low incidence angles provide shallow penetration depth into the sample surface.[26] For selected coating specimens, high temperature x-ray diffraction (HTXRD) measurements were conducted at ORNL using a Scintag PAD X vertical $\theta/2\theta$ goniometer equipped with a modified Buehler HDK-2 diffraction furnace and an MBRAUN Position Sensitive Detector (PSD-50M). All data were collected in vacuum or air. The temperature of the sample heating assembly was measured with a Pt/Pt-10%Rh thermocouple spot-welded to the Pt-30%Rh heater strip on which the sample was placed. The temperature of the surface of the samples was measured with an optical pyrometer (Pyrometer Instrument Company, Inc. Bergenfield, NJ. Model 95).

In addition to XRD, luminescence spectroscopy was used to determine the presence of α-Al_2O_3 in the coating layer and to measure the average stress of the α-Al_2O_3 phase. α-Al_2O_3 has trigonal symmetry with rhombohedral Bravis centering and can possess trace amounts Cr^{3+} cation impurities in the alumina crystal lattice. When excited by a laser, the electrons of the Cr^{3+} cations emit photons.[27] The two characteristic photon energies for the α-Al_2O_3 phase are: 14400 (R1) and 14430 cm^{-1} (R2). A stress in the α-Al_2O_3 phase results in a change in the electronic environment of the Cr^{3+} cations and therefore a corresponding shift in the R1 and R2 lines.[27] A Dilor XY 800 triple stage Raman microprobe and a coherent Innova 308C Argon ion laser operating at 510 nm with a 100 mW output diameter were used. This instrument had a spatial resolution of 2 or 10 µm, depending on the objective used.

Results

SEM/EDS, XRD, and luminescence characterization data suggested that the CVD alumina coating directly deposited on René N5 was essentially made of ~1 µm α–Al_2O_3 crystals in a matrix of amorphous Al_2O_3. Figure 1a shows that the coating surface consisted of two distinct features: (i) faceted crystals of ~0.5-1.5 µm and (ii) a glassy, web-like phase. The coating surface was not fully "dense" due to the lack of coalescence among the crystals as well as the presence of the glassy phase between the crystals. Figure 1b shows that the coating was ~1 µm thick, and contained Al and O only when examined by EDS. The interface at the coating layer and the alloy surface did not appear to be particularly sharp, although the alloy surface was polished to ~0.05 µm before the coating process.

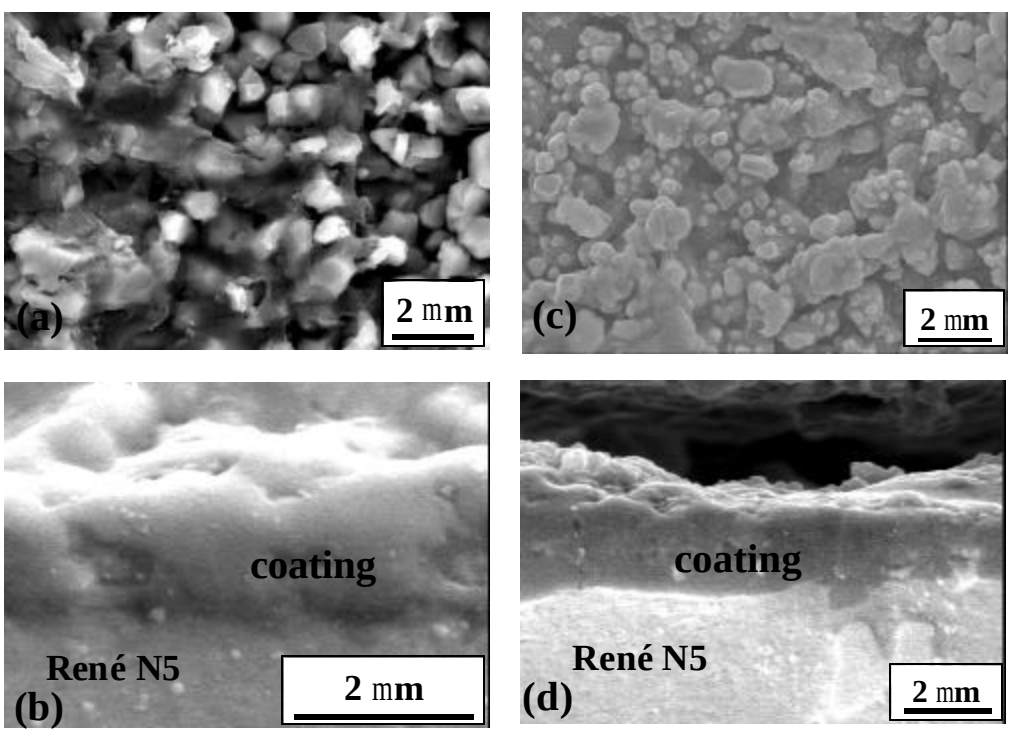

Figure 1. Surface and cross-section images of CVD-Al_2O_3 on René N5:
(a) and (b) as-deposited and (c) and (d) after annealing and oxidation.

The θ-2θ XRD pattern in Figure 2a suggested that the coating contained α-Al_2O_3 crystals that were randomly orientated. The penetration of the XRD beam appeared to be relatively small as the substrate peak was barely visible from the θ-2θ XRD scan, but significant broadening of the

baseline was observed. The high background suggested the presence of some amorphous content within and/or underneath the coating layer, although a more quantitative measure could not be possible with the XRD analysis. The GIXRD scan in Figure 2b showed that the top region of the coating layer was mostly α-Al_2O_3.

As shown in Figure 3, relatively broad R1 and R2 fluorescence peaks were observed for the coating layer with a 10–µm laser probe. A smaller 2–µm probe revealed that the faceted crystals (~0.5-1.5 µm) shown in the SEM micrograph (Figure 1a) were indeed α-Al_2O_3. The R1 and R2 peaks became more intense and shaper as the probe was focused on the crystals. On the other hand, the glassy phase was found to contain neither α- nor θ-Al_2O_3, as evidenced by significant reductions in the intensity of the R1 and R2 peaks. Due to the coefficient of thermal expansion (CTE) mismatch between the α-Al_2O_3 coating and the René N5 substrate, compressive residual stress was expected to develop in the in-plane direction of the coating layer upon cooling from the CVD deposition temperature to room temperature. The average stress in the coating layer was estimated to be –3.2 GPa. However, the broadness of the R1 and R2 peaks suggested a considerable stress distribution in the coating layer.[28]

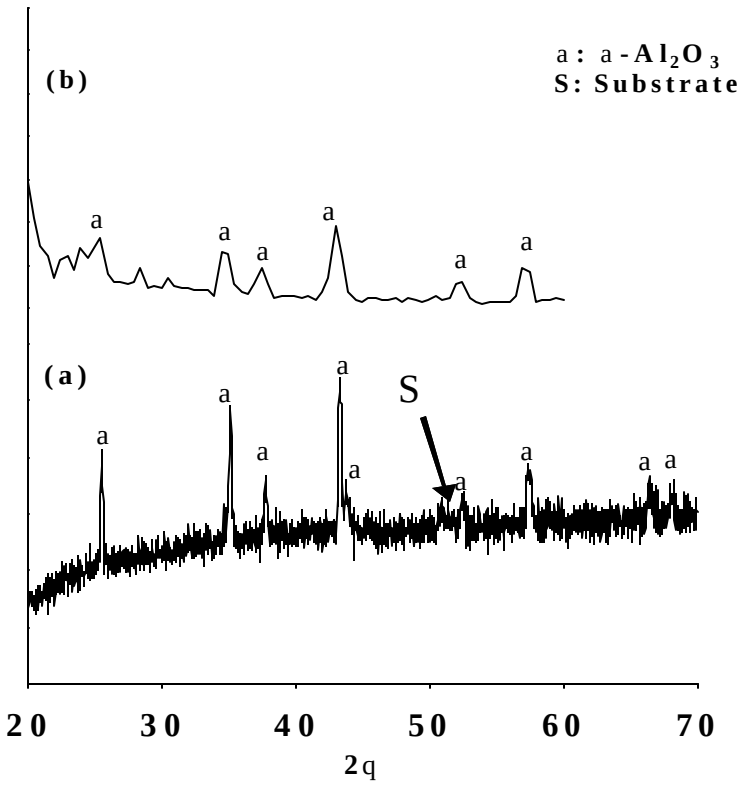

Figure 2. XRD patterns of CVD-Al_2O_3 on René N5: (a) θ-2θ scan and (b) grazing incidence angle of 1°.

The coating deposited on René N5 substrate was annealed in the HTXRD chamber under vacuum as the temperature was gradually increased from 1020 to 1150°C over a period of 2.5 hours. After the sample was cooled to room temperature, it was examined by luminescence spectroscopy and XRD. Subsequently, the same sample was oxidized in the HTXRD chamber in air at 1200°C for 1 hour. Comparison of the SEM micrographs before and after the annealing

and oxidation steps (Figures 1a and 1c) showed the disappearance of the glassy phase observed on the as-deposited surface and the appearance of new small crystallites of ~100 to 500 nm. Also, to a large extent, the original α-Al_2O_3 crystallites (~0.5-1.5 μm) existed on the as-deposited surface appeared to remain, except that some smaller crystallites were observed to grow on the top surface of the large crystallites. The surface morphology appeared denser after the annealing/oxidation steps.

The SEM data indicated that the glassy amorphous Al_2O_3 phase was crystallized during the annealing/oxidation procedures where the coating layer. Comparison of the cross-section SEM micrographs in Figure 1b and 1d suggested that the thickness of the coating layer increased slightly by ~0.5 μm (i.e., the thickness of the CVD-Al_2O_3 layer plus TGO). However, the number of thickness measurements made from various cross-section micrographs was not sufficient enough to make a more quantitative statement about the precise change in the thickness of the coating layer.

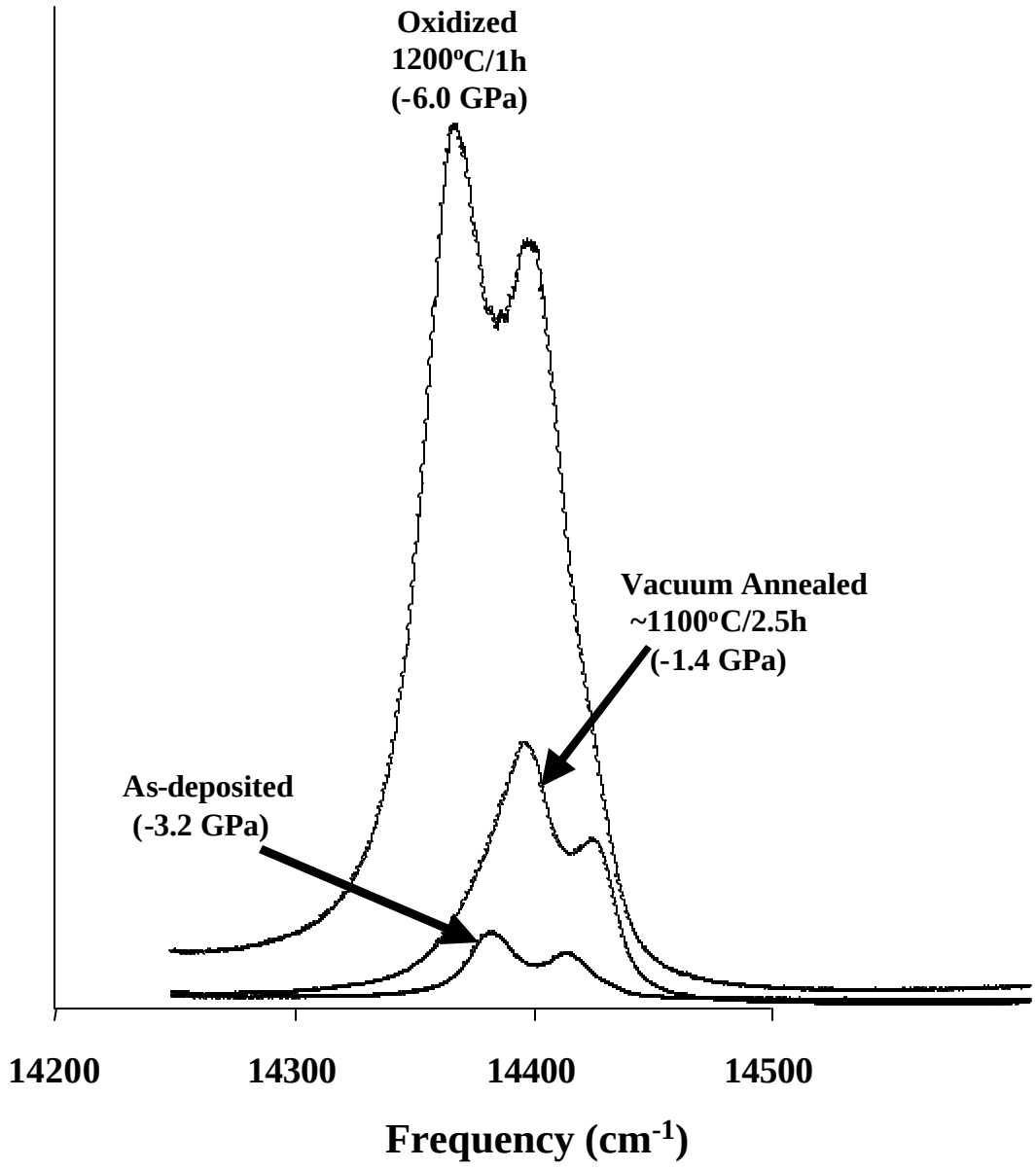

Figure 3. Luminescence spectra of CVD-Al_2O_3 on René N5.

The XRD patterns in Figure 4 supported our interpretation of the SEM results. The amorphous portion of the as-deposited coating layer indeed transformed to α-Al_2O_3 upon the annealing step, as evidenced by the appearance of the stronger α-Al_2O_3 peaks, which seemed to occur at the expense of the high background of the θ-2θ XRD scan. As discussed earlier, the presence of the high XRD background was attributed to the amorphous phase in the as-deposited coating layer. Interestingly, after the annealing step, three intense diffraction peaks appeared. However, we have not been able to assign these peaks yet, despite of significant indexing efforts. After the subsequent oxidation step, the XRD pattern did not change much, except that the unidentified peaks became stronger.

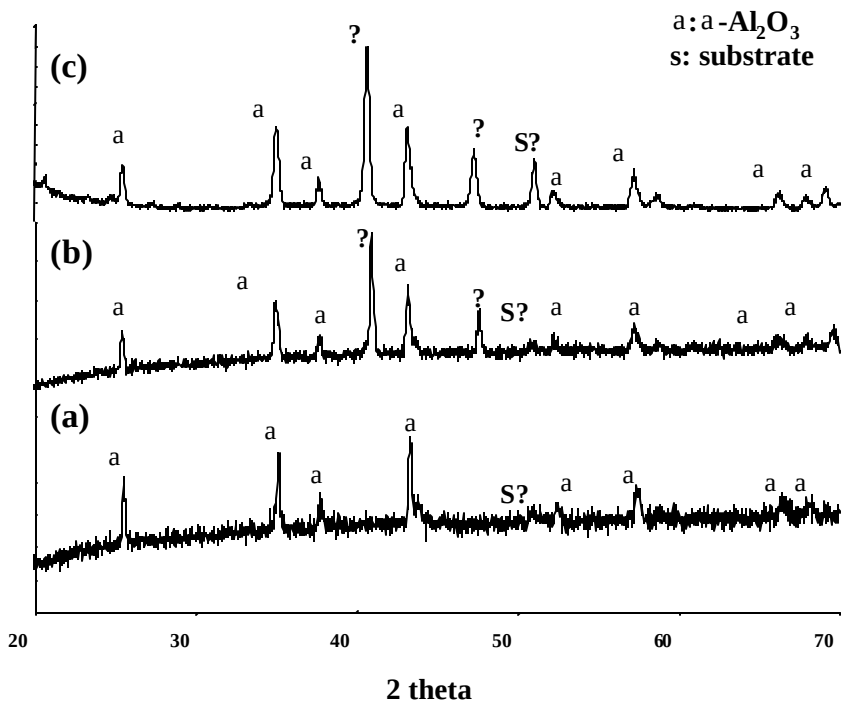

Figure 4. XRD patterns of CVD-Al_2O_3 on René N5: (a) as-deposited, (b) vacuum-annealed at 1020 to 1150°C over a period of 2.5 hours, and (c) oxidized with air at 1200°C for 1 hour.

After the annealing step, the intensity of the R1 and R2 peaks increased as shown in Figure 3. There are two possible explanations for the apparent increase: (1) an increase in the amount of α-Al_2O_3 in the coating layer due to crystallization of the amorphous Al_2O_3 and (2) an increase in Cr^{3+} concentration in the coating layer, as Cr from René N5 might have diffused into the Al_2O_3 layer during the annealing step. The first explanation seemed more consistent with the XRD results. Also, the decrease in the average stress from –3.2 to –1.4 GPa suggested that localized stress relaxation in the Al_2O_3 layer due to microcracking. The microcracking was most likely caused by the crystallization during the annealing step.

After the oxidation step, the R1 and R2 peaks became much more intense and sharpened. The average stress in the coating layer was estimated to be –6.0 GPa. The increases in the peak intensity and average residual stress were attributed to TGO formation. The Cr^{+3} concentration in the TGO was expected to be much higher than in the CVD-Al_2O_3 layer since Cr was present in René N5 as a major alloying element (7 wt%). The luminescence results suggested that the TGO layer was highly stressed. But, at this point, we are not sure about the exact location(s) and

phase(s) of the TGO. TEM studies are currently being conducted to improve our understanding of the apparent annealing and oxidation characteristics.

The surface of the alumina coating deposited on the Pt-Plated René N5 substrate was not uniform, as characterized by the presence of ~20 µm semi-round features (or "rumples") on the coating surface (Figures 5a). On each rumple surface, Al_2O_3 crystals of ~0.1-1 µm were clearly visible (Figure 5b). At higher magnifications, a high density of very fine microcracks (~100 nm) appeared on the coating surface, especially in the "valley" region between the Al_2O_3 crystals (Figure 5c). It has been previously reported that α-Al_2O_3 tended to form as a larger grain surrounded by fine κ-Al_2O_3 grains along with microcracks during CVD.[8] In this regard, the presence of the microcracks could be attributed to the κ to α phase transformation that might have occurred during the CVD process and/or the cooling step.

The coating was ~2 µm thick, and contained small protrusions from the substrate into the coating layer, as indicated by the single arrow in Figure 5d. From the literature in high temperature oxidation, it is known that this type of "pegging" behavior is known to occur during the oxidation of Pt-modified aluminide coatings, and is believed to improve TGO adhesion.[29] Our SEM/EDS analysis did not show the presence of any elements other than Al, O, and Pt in the coating layer. The XRD spectrum showed that the coating was predominately α-Al_2O_3 along with a trace amount of κ-Al_2O_3. In contrast to the coating directly deposited on René N5, the rise in the baseline of the θ-2θ XRD scan was not observed.

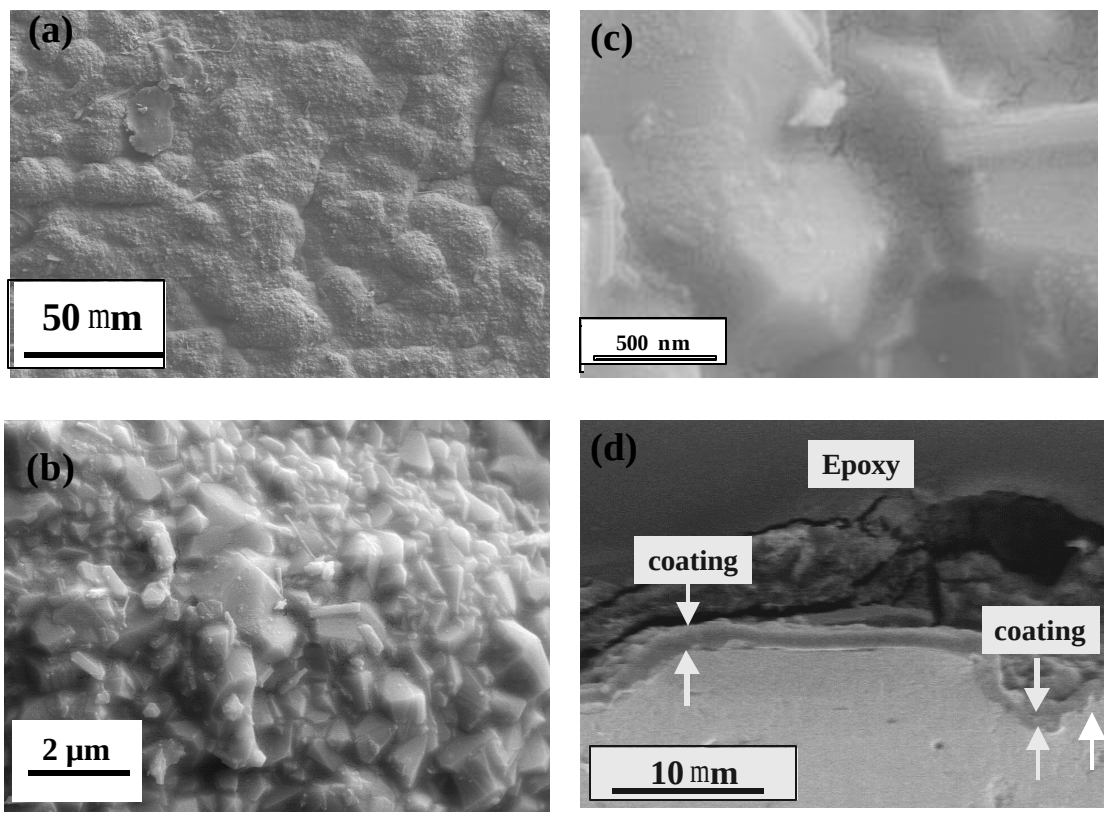

Figure 5. Surface and cross section of as-deposited CVD-Al_2O_3 on Pt-plated René N5.

Surface micrographs in Figure 6a showed that the surface of the coating deposited on pure Pt was highly faceted with hexagonal platelets of ~0.5 μm in size and without any microcracks. Cross-section SEM/EDS analysis showed that the coating layer was ~1 μm thick (Figure 6b), and mainly consisted of Al and O. As in the case of the coating deposited on Pt-plated René N5, protrusions of the metal phase into the coating layer were observed. The majority of the dominant peaks in the θ-2θ XRD scan was indexed to Pt_3Al. A minor amount of κ-Al_2O_3 was detected. Also, significant penetration of Al beneath the κ-Al_2O_3 layer (i.e., into the substrate) was suspected through the formation of Pt_3Al.

The coating was annealed in vacuum for ~2 hours while heating the sample to ~1200°C in the HTXRD chamber. The HTXRD data in Figure 7 show that α-Al_2O_3 formed at the expense of κ-Al_2O_3 between 4 and 12 minutes into the annealing step. In addition to the κ- to α-Al_2O_3 transition, the Pt_3Al peak disappeared as most of the Pt_3Al phase was dissociated back to Pt in about 90 minutes. The results certainly showed that the phase transformation behavior was rather complex. Upon annealing, the faceted surface features of the coating became smoother and more nodular as shown in Figure 6c. The highly faceted, jagged edges observed in the as-deposited cross-section (Figure 6b) became flat after annealing (Figure 6d). The appearance of very fine microcracks (~100 nm) was observed on the entire surface of the coating (Figure 6c). This microcracking behavior was similar to that observed for the coating deposited on Pt-plated René N5 (Figure 5c). Comparison of the cross-section SEM micrographs (Figures 6b and 6d) indicated that there was no significant change in the coating thickness, as a result of the annealing process.

The surface of the alumina coating deposited on pure Ni exhibited a stacked, platelets morphology similar to that deposited on the Pt surface, yet displaying a somewhat more hexagonal shape and a more layered appearance. At high magnifications, the presence of very fine microcracks (~100 nm) was observed from the cross-section view of the coating layer. No crystalline phases of Al_2O_3 were detected by XRD. Most XRD peaks could be indexed to pure Ni and γ'-Ni_3Al. As in the case of the coating directly deposited on René N5, the θ-2θ XRD pattern exhibited a high background, suggesting that there was some amorphous content in the coating. Based on the characterization results, the coating deposited on Ni appeared to be mostly amorphous Al_2O_3. However, it seemed that the very top surface of the coating (~0.4 μm layer) was covered by κ–Al_2O_3 platelets, as evidenced by their hexagonal plate morphology.[21]

Discussion and Conclusions

As evident from widely varying surface morphologies observed in the present study, the results clearly showed the strong effects of substrate on the phase content and morphology of the CVD-Al_2O_3 coating. The coating deposited on René N5 mainly consisted of α-Al_2O_3 crystals in a matrix of amorphous Al_2O_3. On the other hand, the alumina coating formed on pure Ni appeared to be mostly amorphous. Therefore, one common feature observed for the René N5 and Ni substrates was the presence of amorphous Al_2O_3 in the coating layer. In comparison, the presence of amorphous Al_2O_3 was not evident from the coatings deposited on pure Pt and Pt-plated René N5 substrates. These observations implied that Ni in the René N5 and Ni substrates favored the formation of the amorphous phase, while certain alloying elements from the René N5 might have promoted the nucleation of α-Al_2O_3.

In contrast to the René N5 and Ni substrates, the XRD results indicated that the coatings deposited on pure Pt was predominantly κ-Al_2O_3, whereas α-Al_2O_3 was the dominant phase on the Pt-plated René N5 surface. Microcracks observed on the surface of the coating deposited on

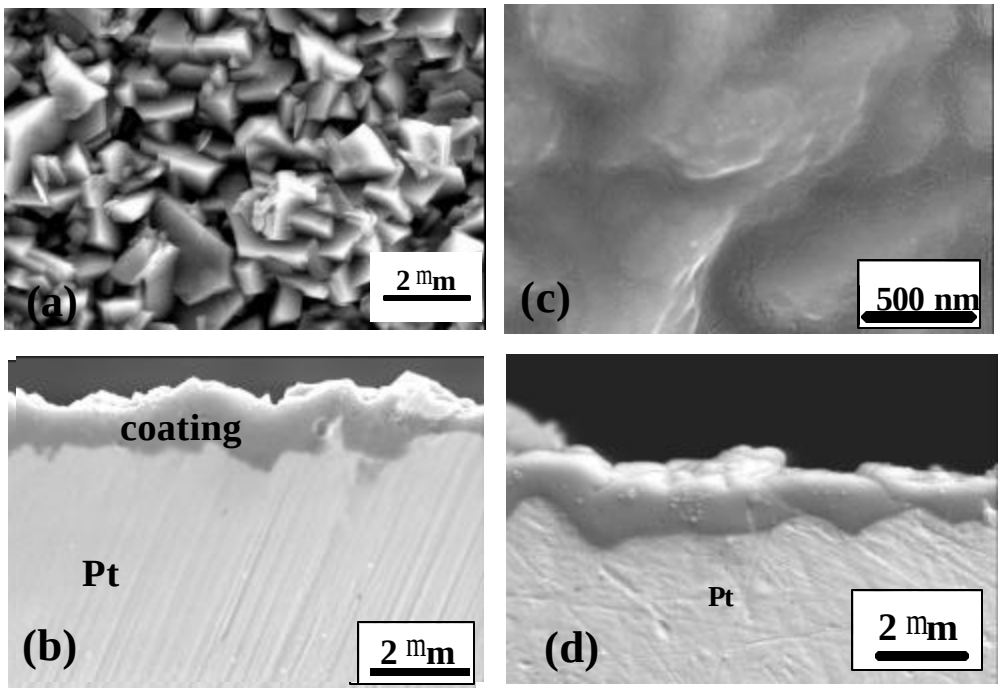

Figure 6. Surface and cross-section images of CVD-Al_2O_3 on pure Pt: (a) and (b) as-deposited and (c) and (d) after annealing

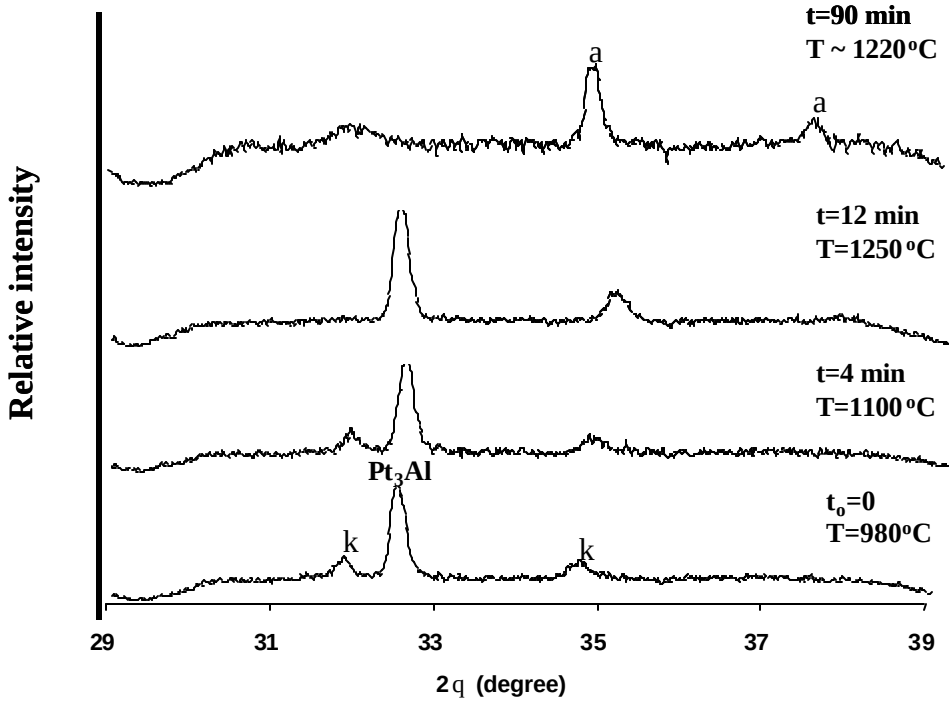

Figure 7. HTXRD patterns of CVD-Al_2O_3 on pure Pt as a function of annealing time.

the Pt-plated Ni superalloy (Figure 5c) suggested that κ– to α-Al_2O_3 phase transformation had already occurred during the CVD process. The microcracking most likely occurred as a result of the volume shrinkage associated with the κ- to α-Al_2O_3 phase transformation (i.e., κ- and α-Al_2O_3 densities are 3.98 and 3.99 g/cm^3, respectively).[30] On the other hand, the coating deposited on the pure Pt substrate remained as κ-Al_2O_3 during the CVD process. However, the coating rapidly transformed to α-Al_2O_3 along with the appearance of a similar microcracking behavior upon annealing.

The results from the Pt-plated René N5 and pure Pt substrates suggested that the major role of Pt was perhaps the nucleation of κ-Al_2O_3 at the early stage of the CVD coating process. Furthermore, it appeared that certain alloying elements from the René N5 might have promoted the formation of some α-Al_2O_3 nuclei on the Pt-plated René N5 surface, as in the case of the coating directly deposited on the René N5 surface. This would result in the seeding and acceleration of the κ- to α-Al_2O_3 phase transformation process, while the coating layer was growing in the CVD reactor. This interpretation implied that α–Al_2O_3 nuclei did not form on the pure Pt surface during the CVD deposition process.

It was interesting to observe rather rapid formation of the Pt_3Al reaction layer between the κ–Al_2O_3 layer and the pure Pt substrate. However, the formation of the Pt_3Al phase was not evident from the Pt-plated René N5 substrate. It has been previously reported that Pt is capable of Al uptake during oxidation[31] and/or CVD processes as will be described later. Also, the presence of protrusions (or pegging) at the coating-substrate interface observed for both pure Pt and Pt-plated René N5 substrates was intriguing since a similar behavior was observed during the oxidation of Pt-modified aluminide coatings. This phenomenon has been considered as one of the beneficial effects of Pt on TGO adhesion.

In summary, the results from the present study suggested that the nucleation and growth of a fully α-Al_2O_3 layer on the Ni superalloy surface, without forming microcracks, would be difficult through simple adaptation of the CVD process previously developed for the cutting tool industry. Currently, we are exploring the extent of morphological tailoring, that may be possible via proactive control of nucleation behavior and alloy surface modifications, using an experimental CVD reactor at Stevens.

Aknowledgements

This research was sponsored by the U.S. Office of Naval Research (ONR) through Grant N00014-99-1-0281. We are grateful to Dr. Steve Fishman at ONR for his support and encouragement. We also thank Dr. Ram Darolia at GEAE who has provided an industrial perspective on our reesearch goal and progress. The HTXRD and luminescence studies were sponsored by the U. S. Department of Energy, Office of Basic Energy Sciences, Division of Materials Sciences and Engineering, and through the High Temperature Materials Laboratory User Program sponsored by the DOE Office of Transportation Technologies under contract DE-AC05-00OR22725 with UT-Battelle, LLC Oak Ridge National Laboratory. J. D. Meyer and M. Torzilli were supported by the Robert C. Stanley Fellowships at Stevens.

References

1. J.T. DeMasi-Marcin and D.K. Gupta, Surf. Coat. Tech., **68/69** (1994) 1-9.
2. R.V. Hillery, et al., "Coatings for High Temperature Structural Materials: Trends and Opportunities," National Academy Press, Washington, DC (1996).

3. W.Y. Lee, D.P. Stinton, C.C. Berndt, F. Erdogan, Y.D. Lee, and Z. Mutasim, J. Am. Ceram. Soc., **79** (1996) 3003-3012.
4. S.M. Meier, D.M. Nissley, K.D. Sheffler, and T. A. Cruse, Trans ASME, **114** (1992) 258-263.
5. E.C. Duderstadt and B. A. Nagaraj, U.S. Patent (1993) No. 5,238,752.
6. T.E. Strangman, U.S. Patent, (1990) No. 4,880,614.
7. J.H. Sun, E. Chang, C.H. Chao, and M. J. Cheng, Oxid. Metals, **40** (1993) 465-481.
8. E. Fredriksson and O.-J. Carlsson, J. Chem. Vapor Dep., **1**, (1993) 333-417.
9. M.K. Smit, G.A. Acekt, and C.J. van de Lann, Thin Solid Films, **138** (1986) 171-181.
10. H.K. Pulker, W. Haag, M. Buhler, and E. Moll, J. Vac. Sci. Technol. A., **3** (1985) 2700-2701.
11. T.C. Chou, D. Adamson, J. Mardinly, and T.G. Nieh, Thin Solid Films, **205** (1991) 131-139.
12. A. Feldman, E.N. Farbaugh, and Y.N. Sun, Optical Society of America Technical Digest Series 6 (1988) 14-17.
13. R.S. Bhattacharya, A.K. Rai, and A.W. McCormick, Surf. Coat. Technol., **46** (1991) 155-163.
14. M.S. Al-Robaee, M.G. Krishna, G. N. Subanna, K. N. Rao, and S. Mohan, J. Mater. Res., **9** (1994) 2668-2694.
15. T.D. Schemmel, R.L. Cunningham, and H. Randhawa, Thin Sold Films, **181** (1989) 597-601.
16. M. Halvarsson and S. Vuorinen, Surf. Coat. Technol., **76/77** (1995) 287-296.
17. H. Alltena, C. Colombier, A. Lebl, J. Lindström, and B. Lux, Proc. 4th Euro. Conf. CVD, edited by J. Bloem et al. (1983) 428-434.
18. Y. Zang, W.Y. Lee, J.A. Haynes, I.G. Wright, B.A. Pint, K.M. Cooley, and P.K. Liaw, Metall. Trans. A, **30A** (1999) 2679-2687.
19. J.A. Haynes, Y. Zhang, W.Y. Lee, B.A. Pint, I.G. Wright, and K.M. Cooley, in Elevated Temperature Coatings: Science and Technology III, The Minerals, Metals, and Materials Society, edited by J. M. Hampikian and N. B. Dahotre (1999) 185-196.
20. H. Altena, C. Colombier, and B. Lux, Proc. 4th Euro. Conf., edited by J. Bloem et al. (1983) 451-458.
21. B. Lux, C. Colombier, H. Altena, and K. Stjernberg, Thin Solid Films, **138** (1986) 49-64.
22. S. Ruppi, U.S. Patent (1992) No. 5,137,774.
23. Y.-F. Su et al., unpublished results.
24. I.G. Wright, P.A. Pint, W.Y. Lee, K.B. Alexander, and K. Prüßner, in High Temperature Surface Engineering, Institute of Materials (in press) 95-113.
25. B.A. Pint, I.G. Wright, W.Y. Lee, Y. Zhang, K. Prüßner, and K. B. Alexander, "Substrate and Bond Coat Compositions: Factors Affecting Alumina Scale Adhesion," Mater. Sci. Eng. A, **245** (1998) 201-211.
26. A.J. Perry, D.E. Geist, A.F. Tian, J.R. Treglio, and K. Narasimhan, Surf. Coat. Technol., **89** (1997) 62-69.
27. G. Gregori, W. Burger, and V. Sergo, Mat. Sci. Eng. A, **271** (1999) 401-406.
28. D.R. Clarke, R.J. Christensen, and V.T. Tolpygo, Surf. Coat. Technol., **94-95** (1997) 89-93.
29. Y. Zhang, Ph.D. Thesis, University of Tennessee, Knoxville, Tennessee (1998).
30. I. Levin and D. Brandon, J. Am. Cerm. Soc., **81** (1998) 1995-2012.
31. G.R. Krishna, D.K. Das, V. Singh, and S.V. Joshi, Mater. Sci. Eng. A, **251** (1998) 40-47.